Original Paper

Indoor and Built Environment

Indoor and Built Environment
0(0) 1–13

DOI: 10.1177/1420326X16662509
ibe.sagepub.com

SAGE

Investigation of particle deposition efficiency enhancement in turbulent duct air flow by surface ribs with hybrid-size ribs

Hao Lu and Lin Lu

Abstract

This study presents the particle deposition enhancement by hybrid-size and same-size surface ribs in turbulent air duct flows using computational fluid dynamics simulation. The Reynolds stress turbulence model with UDF corrections and discrete particle model were adopted to simulate the turbulent air flow fields and particle deposition behaviours, respectively. After numerical validation with the relative literature results, pure particle deposition enhancement ratios, flow drag increase, comprehensive deposition efficiency and deposition enhancement mechanisms were investigated and discussed in details. The findings showed that the hybrid-size ribs with small rib spacing have the best enhancement performance on particle deposition for small particles ($\tau_p^+ < 1$). Considering the flow drag increase, the maximum deposition efficiency can reach 485 for 1 μm particles for the hybrid-size ribbed cases, while it is just 425 for the same-size ribbed case. Nevertheless, no obvious particle deposition enhancement can be found for large particles ($\tau_p^+ > 1$) for all types of surface ribs. The hybrid-size surface ribs are more efficient compared with the same-size ribs, which can be applied in the air cleaning equipment to improve the aerosol particle removal performance.

Keywords

Particle deposition, Efficiency enhancement, Hybrid-size rib, Computational fluid dynamics, Numerical simulation

Accepted: 10 July 2016

Introduction

The efficiency and performance of the air clean devices are important consideration, as air pollution has become a serious problem in urban environment and aerosol particulate matters could cause extreme damages to people's health.[1,2] The arrangement of surface ribs on the air electrostatic precipitators (ESP) can greatly improve the performance of the aerosol particle removal efficiency, as a large number of aerosol particles would be intercepted by the windward of surface ribs.[3] Lai et al.[4,5] experimentally found that the particle deposition rate in duct air flow would be obviously enhanced by surface ribs. Nevertheless, the flow drag of the air flow would be also increased at the same time due to the form drag of the surface ribs, which means more energy should be consumed for driving the airflow. Therefore, the design of optimized surface rib parameters is essential and crucial to improve the particle removal efficiency with low flow drag.

However, the studies on particle deposition enhancement in turbulent air flow by surface ribs are limited. For experimental study, Lai et al.[4,5] experimentally investigated aerosol particle loss enhancement in ventilation duct by two-dimensional (2D) and three-dimensional (3D) ribbed surfaces. The results showed that the

Department of Building Services Engineering, The Hong Kong Polytechnic University, Hung Hom, Kowloon, Hong Kong, China

Corresponding author:
Lin Lu, Department of Building Services Engineering, The Hong Kong Polytechnic University, Room ZS850, Block Z, Hung Hom, Kowloon, Hong Kong.
Email: vivien.lu@polyu.edu.hk

arrangement of surface ribs can be applied to improve the performance of current air filtration device. Moreover, Barth et al.[6] studied multilayer particle deposition and re-suspension in turbulent channel flow by particle image velocimetry system (PIV) combined with gravimetrical and X-ray methods. The multilayer particle deposition process was found to be significantly influenced by inertia impaction, gravitational settling and turbulent dispersion. Compared with experimental study, numerical simulation based on computational fluid dynamics (CFD) method has been generally used as a powerful tool to investigate and predict particle deposition and behaviour in turbulent air flow.[7–9] Suh and Kim[10] numerically predicted particle collection efficiency in obstructed passage for ESP by standard $k-\epsilon$ turbulent model and trajectory method. The results indicated that the obstructions can greatly increase the collection efficiency for smaller particles. Iacono et al.[11] compared the influence of surface ribs on particle deposition process with different particle shapes by large eddy simulation (LES). Cylindrical particle behaviours were shown to be obviously different with those for spherical particles. Lecrivain et al.[12] numerically investigated multilayer particle deposition in turbulent duct air flow with ribbed surface. The results showed that the CFD prediction was in good agreement with the experimental data.

In our previous studies, the enhancement effects and mechanisms,[13] the effects of rib spacing and height,[14] the effects of rib shapes[15] and the effects of rib arrangement[16] on particle deposition in duct air flows were investigated systematically. The objective of our previous studies was to investigate the optimal rib parameters and arrangements for higher particle deposition enhancement with lower flow drag increase. Our results had shown that the square shape ribs with smaller heights and spacing can enhance the particle deposition rate better with lower flow drag increase. Moreover, the results showed that the turbulence eddies induced by the surface ribs could play an important role on the particle deposition enhancement, especially for small particles. Nevertheless, for better performance of high particle deposition enhancement with low flow drag, more efforts for optimal configurations of surface ribs should be conducted. Recently, Xie et al.[17] numerically investigated the heat transfer enhancement in a square channel by surface ribs with combined same-size or half-size ribs. Their results implied that the hybrid-size surface ribs can enhance heat transfer better with lower flow drag increase. Nevertheless, the efficiency performance of the hybrid-size surface ribs on particle deposition has never been investigated. Therefore, there is a need to investigate the efficiency and mechanism of the hybrid-size surface ribs on particle deposition enhancement. This study aims to numerically investigate the particle deposition rate in turbulent duct airflow with hybrid-size surface ribs. Instead of numerical method, the novelty of this study is to focus on the hybrid-size surface ribs, so the reliable numerical models (RSM and DPM model), which had been successfully applied in our previous studies, were also adopted in this study. The particle deposition velocity and flow drag for hybrid-size ribbed duct cases were investigated in details and compared with those for the same-size ribbed duct cases. Moreover, the mechanisms of particle deposition enhancement for different particle sizes in hybrid-size and same-size ribbed duct air flows were analysed and discussed.

Numerical model and methodology

Turbulent air flow model

To simulate the gas-particle flow in smooth and ribbed ducts, the Reynolds stress model (RSM) with velocity fluctuation correction and discrete particle model (DPM) were employed to predict turbulent airflow fields and particle deposition behaviour, respectively. The commercial CFD software ANSYS Fluent 13.0 with UDF codes was employed for the simulation. The mass and momentum conservation governing equations[18] and Reynolds stress transport equation[18] for turbulent airflow are demonstrated by equations (1) to (3), as follows[18]

$$\frac{\partial \overline{u}_i}{\partial x_i} = 0 \tag{1}$$

$$\frac{\partial \overline{u}_i}{\partial t} + \overline{u}_j \frac{\partial \overline{u}_i}{\partial x_j} = -\frac{1}{\rho}\frac{\partial \overline{p}}{\partial x_i} + \frac{1}{\rho}\frac{\partial}{\partial x_j}\left(\mu \frac{\partial \overline{u}_i}{\partial x_j} - \rho \overline{u_i' u_j'}\right) \tag{2}$$

$$\begin{aligned}\frac{\partial}{\partial t}\left(\overline{u_i' u_j'}\right) + \bar{u}_k \frac{\partial}{\partial x_k}\left(\overline{u_i' u_j'}\right) &= \underbrace{\frac{\partial}{\partial x_k}\left(\frac{\nu_t}{\sigma_k}\frac{\partial \overline{u_i' u_j'}}{\partial x_k}\right)}_{D_{T,ij}=\text{Turbulent Diffusion}} \underbrace{-\left(\overline{u_i' u_k'}\frac{\partial \bar{u}_j}{\partial x_k} + \overline{u_j' u_k'}\frac{\partial \bar{u}_i}{\partial x_k}\right)}_{P_{ij}=\text{Stress Production}} \\ &\underbrace{-C_1\frac{\varepsilon}{k}\left[\overline{u_i' u_j'} - \frac{2}{3}\delta_{ij}k\right] - C_2\left[P_{ij} - \frac{2}{3}\delta_{ij}P\right]}_{\phi_{ij}=\text{Pressure Strain}} - \underbrace{\frac{2}{3}\delta_{ij}\varepsilon}_{\varepsilon_{ij}=\text{Dissipation}}\end{aligned} \tag{3}$$

where $\bar{u}_i$, $\bar{p}$ and $\rho\overline{u_i' u_j'}$ are the time-averaged velocity, the time-averaged pressure and the Reynolds stress tensor, respectively.

The two-layer zonal model with enhanced wall function was adopted to accurately resolve the turbulent air flow fields near the wall.[18,19] The near-wall turbulent

velocity fluctuation is crucial for accurate prediction of particle deposition velocity.[20,21] To improve the simulation accuracy, the wall-normal turbulent velocity fluctuation profiles obtained from direct numerical simulation (DNS) data were adopted to correct the RSM results by UDF codes. For smooth duct case, the turbulent velocity fluctuation was corrected as illustrated by equation (4) according to the DNS data by Kim et al.[22]

$$\frac{v'_{rms}}{u^*} = C(y^+)^2, \quad \text{for } y^+ < 4 \tag{4}$$

For ribbed duct flow, the correction equation for near-wall turbulent velocity fluctuation is represented by equation (5) as follows[12]

$$\frac{v'_{rms}}{u^*} = \frac{a_1 y^{+2}}{1 + b_1 y^+ + c_1 y^{+2.41}}, \quad \text{for } y^+ < 30 \tag{5}$$

where u^* is the friction velocity. $C = 0.008$, $a_1 = 0.0116$, $b_1 = 0.203$ and $c_1 = 0.0014$. y^+, the non-dimensional distance from the wall, is defined by equation (6) as follows

$$y^+ = \frac{y\, u^*}{\nu} \tag{6}$$

To make sure full development of turbulent duct air flow, the velocity profiles of one seventh power law were imposed in the air inlet by UDF codes. The fully developed velocity profiles[20] are defined by equations (7) to (9) as follows

$$U = U_{free}\left(\frac{y}{D/2}\right)^{1/7} \quad \text{for} \quad y \le D/2 \tag{7}$$

$$U = U_{free}\left(\frac{h-y}{D/2}\right)^{1/7} \quad \text{for} \quad y > D/2 \tag{8}$$

$$U_{free} = \frac{8}{7} U_{mean} \tag{9}$$

where D and U_{mean} are the duct height and the mean air velocity, respectively. Moreover, the fully developed turbulent kinetic energy (T.K.E.) profiles were computed and imposed at the duct inlet as illustrated by equations (10) to (12).[20]

$$k = \frac{\tau_w}{\rho_g\sqrt{C_\mu}} + \frac{y}{D/2}\left(0.002U_{free}^2 - \frac{\tau_w}{\rho_g\sqrt{C_\mu}}\right) \quad \text{for} \quad 0 \le y \le D/2 \tag{10}$$

$$k = \frac{\tau_w}{\rho_g\sqrt{C_\mu}} + \frac{D-y}{D/2}\left(0.002U_{free}^2 - \frac{\tau_w}{\rho_g\sqrt{C_\mu}}\right) \quad \text{for} \quad D/2 < y \le D \tag{11}$$

$$\tau_w = \frac{\rho_g U_{mean}^2}{2} \cdot f \tag{12}$$

Particle motion model

DPM was employed to simulate particle dispersion and deposition behaviours. As the gas-particle flows considered in the present study are dilute enough and the air velocity is low, the below assumptions can be made in the simulation[23–25]

1. The influence of particle phase on turbulent air flow can be neglected;
2. The inter-particle collisions are not considered here;
3. The particles would not be rebound and re-suspended from the walls or rib surfaces.

Considering the drag force, the gravity force, the buoyancy force, the Brownian force and the Saffman's lift force, the particle motion governing equation is illustrated by equation (13) as follows

$$\frac{du_p}{dt} = \frac{1}{\tau}\frac{C_D \mathrm{Re}_p}{24}(u_g - u_p) + \frac{g(\rho_p - \rho_g)}{\rho_p} + \zeta\sqrt{\frac{\pi S_0}{\Delta t}} + \frac{2\rho K_c \nu^{0.5}}{\rho_p d_p (S_{lk}S_{kl})} s_{ij}(u - u_p) \tag{13}$$

where u_g and u_p are the air and particle velocities, respectively. ρ_g and ρ_p is air density and particle density, respectively. The pressure gradient force, the Basset force and the virtual mass force can be neglected compared with the external forces of particles, as the ratio of air density to particle density is very small.[26–28] The drag coefficient, C_D, can be computed as given by equations (14) and (15)

$$C_D = \frac{24}{\mathrm{Re}_p}, \quad \text{for } \mathrm{Re}_p < 1 \tag{14}$$

$$C_D = \frac{24}{\mathrm{Re}_p}(1 + 0.15\mathrm{Re}_p^{0.687}), \quad \text{for } 1 < \mathrm{Re}_p < 400 \tag{15}$$

The particle relaxation time, τ, can be computed as defined by equation (16)

$$\tau = \frac{S d_p^2 C_C}{18\nu} \tag{16}$$

where S is the ratio of particle density to fluid density and C_C is the Cunningham slip correction factor.

The particle deposition behaviours could be extremely influenced by particle turbulent dispersion.[20] In this present study, turbulent dispersion of particles was simulated by discrete random walk (DRW) model. The DRW model is characterized by a Gaussian distributed random velocity fluctuation of fluids and a time scale of turbulent eddy.[18] In RSM model, the instantaneous turbulent velocity fluctuation can be calculated by equation (17)

$$u' = \zeta u'_{rms}, \quad v' = \zeta v'_{rms}, \quad w' = \zeta w'_{rms} \qquad (17)$$

where u'_{rms}, v'_{rms} and w'_{rms} are the velocity fluctuation. ζ is a zero mean, unit variance normally distributed random number.[20] In the DRW model, the turbulent fluctuation velocity is produced by the normal distributed random number ζ and the root mean square (RMS) fluctuation velocity.

In the calculation, the 'Escape' condition was adopted at duct inlet and outlet for particles. Moreover, the 'Trap' condition was employed on the walls and rib surfaces for particle phase.[29–31] The 'Trap' condition means that the particle would be deposited once it contacts with the duct walls or rib surfaces. In this study, the rebound and re-suspended behaviours were not considered.

Case description and solution methods

Figure 1 shows the two-dimensional (2D) smooth and ribbed ducts in the simulation. The smooth duct was established according to the geometry configuration in the literature[20,21] for comparison, which is 0.4 m long

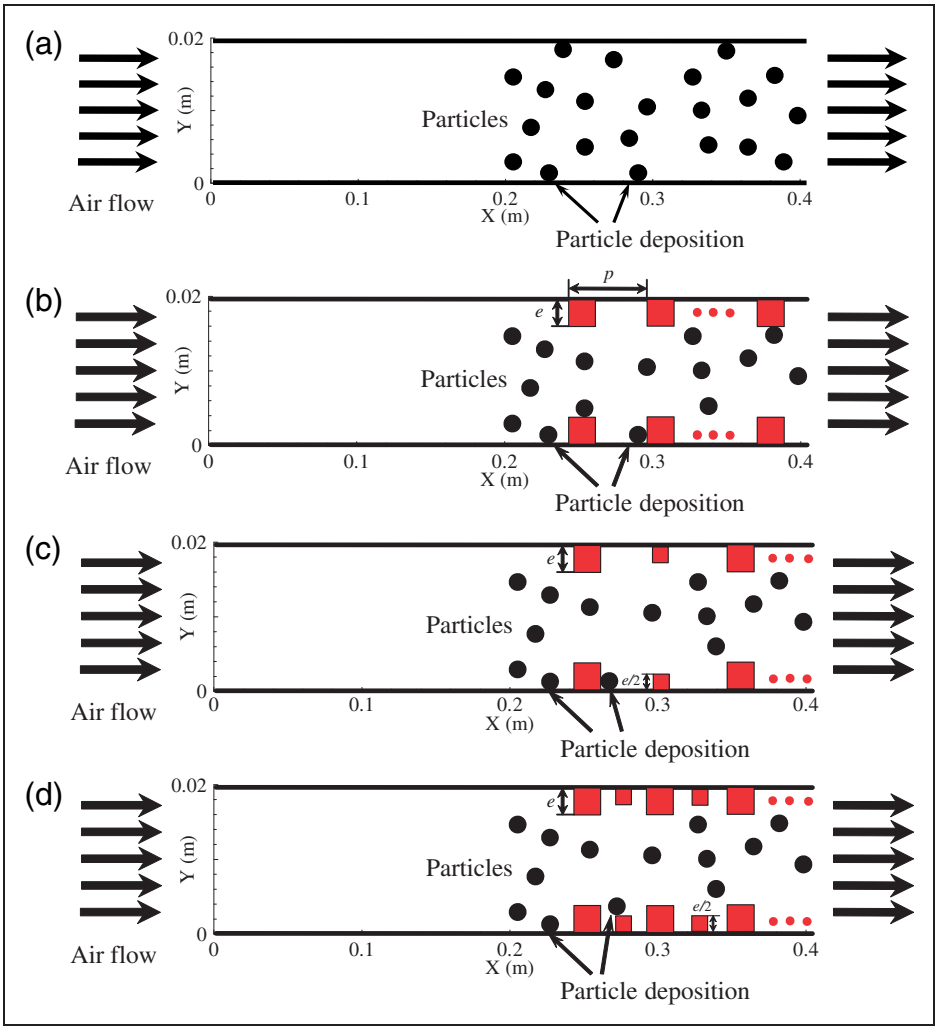

Figure 1. Schematic of particle air flow in smooth, same-size and hybrid-size ribbed ducts. (a) Smooth-wall duct, (b) ribbed-wall duct, case A, (c) ribbed-wall duct, case B, (d) ribbed-wall duct, case C.

and 0.02 m high. Three types of ribbed ducts were designed to enhance particle deposition rate: the same-size surface ribs with a pitch ratio of $p/e = 10$ (ribbed case A), the hybrid same-size and half-size surface ribs with a pitch ratio of $p/e = 10$ (ribbed case B), and the hybrid same-size and half-size surface ribs with a pitch ratio of $p/e = 5$ (ribbed case C), as shown in Figure 1(b) to (d), respectively. The height of same-size surface rib is: $e = 0.1$ D and 0.05 D for half-size surface ribs. D is the duct height. The first half of the ribbed duct was designed as smooth to ensure the fully developed turbulent air flow, while the second half of the ribbed duct was arranged by surface ribs with the same rib spacing. In the present study, the following parameters were considered: air velocity, 5.5 m/s, air dynamic viscosity μ, 1.789×10^{-5} kg s/m and air density, 1.225 kg/m^3 at $T = 288$ K. Therefore, the Reynolds number of the air flow based on the mean velocity and duct height was 7534. After the turbulent air, flow fields were calculated to be convergent, 30,000 spherical particles were released into the flow fields at the streamwise position $X = 0.2$. The initial particle velocities were equal to the mean air velocity. The density ratio of particle to fluid S was 2000 and the gravity force was parallel with the air flow direction. The particle sizes were 1, 2, 3, 5, 10, 20, 30 and 50 μm. Therefore, a total number of 32 cases were investigated in the present study as shown in Table 1.

The structured grids were developed to discretize the computational domain for smooth and ribbed duct cases by using Ansys ICEM 13.0. Tian and Ahmadi[20] studied the influence of computational grid solution on the predicted results of particle deposition in smooth duct. The results showed that the accurate deposition velocities can be obtained when the first grid spacing is 0.05 mm with a grid growing factor of 1.2 from the walls to the core regions. Their first grid spacing was about 1.13 in wall units. Therefore, in this study, the grid independence check was not conducted repeatedly. The first grid spacing from the walls and rib surfaces was selected as 0.05 mm. The grid growing factor was 1.2 from the walls and rib surfaces to the core regions.[20] The grid numbers for smooth duct and three types of ribbed duct cases were: 32000, 101251, 98415 and 97021, respectively. The partial structured grids in the calculation for the four ducts are displayed in Figure 2(a) to (d).

The finite volume method (FVM) was employed to solve the turbulent air flow governing equations. The convection term was discretized by the second-order upwind scheme. The diffusion term was discretized by the second-order central difference scheme. The SIMPLE algorithm[32] was adopted to decouple the pressure and velocity fields. The Runge–Kutta method was employed to resolve the particle motion equations. The correction of turbulent velocity fluctuations as well as the inlet velocity and T.K.E. profiles were imposed into FLUENT by UDF codes.

Results and discussion

Air duct flow fields and numerical validation

Figure 3 shows instantaneous air velocity fields for smooth and ribbed duct cases. For smooth duct case, turbulent boundary layer can be clearly observed, as shown in Figure 3(a). For ribbed duct cases, the near-wall flow structures are significantly modified by the surface ribs. The periodic recirculation zones are induced in the cavities between the near-by surface ribs and the turbulent boundary layers are shifted away from the walls due to the disturbance of the surface ribs. Therefore, the flow fields in the near wall regions for the ribbed duct cases are more complicated, compared with the smooth duct case. From the figure, the turbulent air flow fields are shown to be resolved reasonably and correctly.

To further validate the air flow velocity profiles in the simulation for the smooth and ribbed duct cases, Figure 4(a) and (b) give the air flow velocity profiles obtained at $X = 0.3$ m for smooth duct case and air velocity profiles in 10 streamwise positions from the 8th and 9th surface ribs for ribbed duct case A, respectively. For the smooth duct case, the results obtained in the present simulation were compared with the DNS data by Kim et al.,[22] as shown in Figure 4(a). The present flow velocity profile was shown in good agreement

Table 1. Computational cases.

Case No.	Air velocity (m/s)	Particle diameter (μm)	Surface type	Rib arrangement	Rib spacing p/e
S (1–8)	5.5	1,2,3,5,10,20,30,50	Smooth	–	–
A (9–16)	5.5	1,2,3,5,10,20,30,50	Ribbed	Same-size	10
B (17–24)	5.5	1,2,3,5,10,20,30,50	Ribbed	Hybrid-size	10
C (25–32)	5.5	1,2,3,5,10,20,30,50	Ribbed	Hybrid-size	5

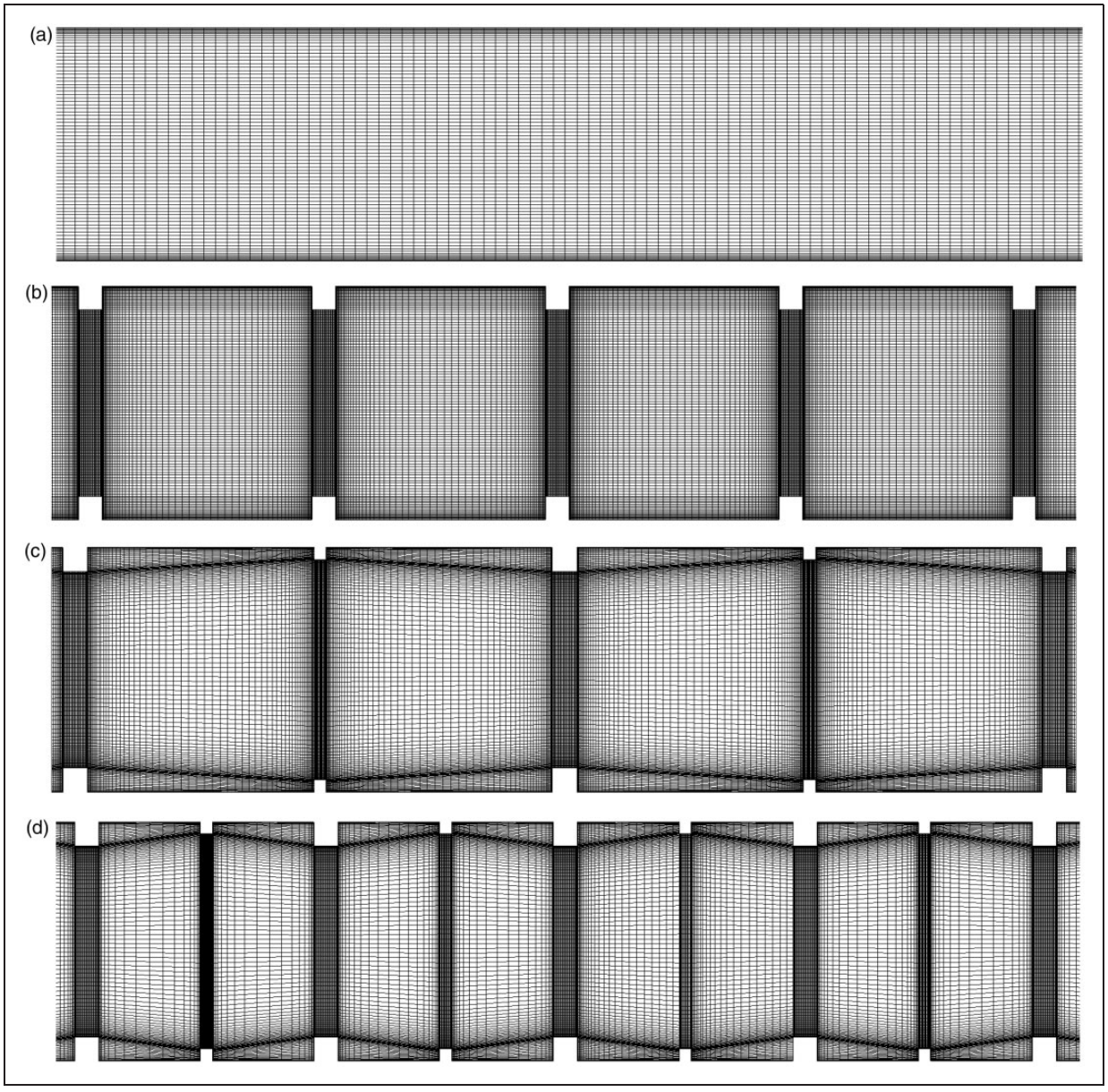

Figure 2. Structural grids for smooth, same-size and hybrid-size ribbed ducts. (a) Smooth-wall duct, (b) ribbed-wall duct, case A, (c) ribbed-wall duct, case B, (d) ribbed-wall duct, case C.

with the DNS results. For the ribbed duct case, Casarsa[33] experimentally measured the air velocity distributions in the cavity between two nearby surface ribs. Although the surface rib parameters are $e/D = 0.3$ and $p/e = 10$ in the experiments, the surface rib parameters are $e/D = 0.1$ and $p/e = 10$ in our present study. Considering the pitch ratio of rib is the most important parameter to determine the flow velocities distributions in the cavity, the experimental data from Casarsa were also adopted to validate the present CFD simulation, as no completely same experimental data of air flow velocities can be found from the literatures. The present velocity profiles were shown to agree well with the experimental measurement from the figure. The above verifications have therefore validated the present RSM model with turbulent fluctuation correction which can resolve the turbulent air flow fields well for both smooth and ribbed duct cases.

Further, the dimensionless particle deposition velocity for smooth duct case was calculated and verified with the literature results,[20,21,34–41] as shown in Figure 5. The particle deposition velocity was computed as given by Equation (18) as follows[20,21]

$$V_d = \frac{J}{C_0} = \frac{N_d/t/A}{N_0/V} \tag{18}$$

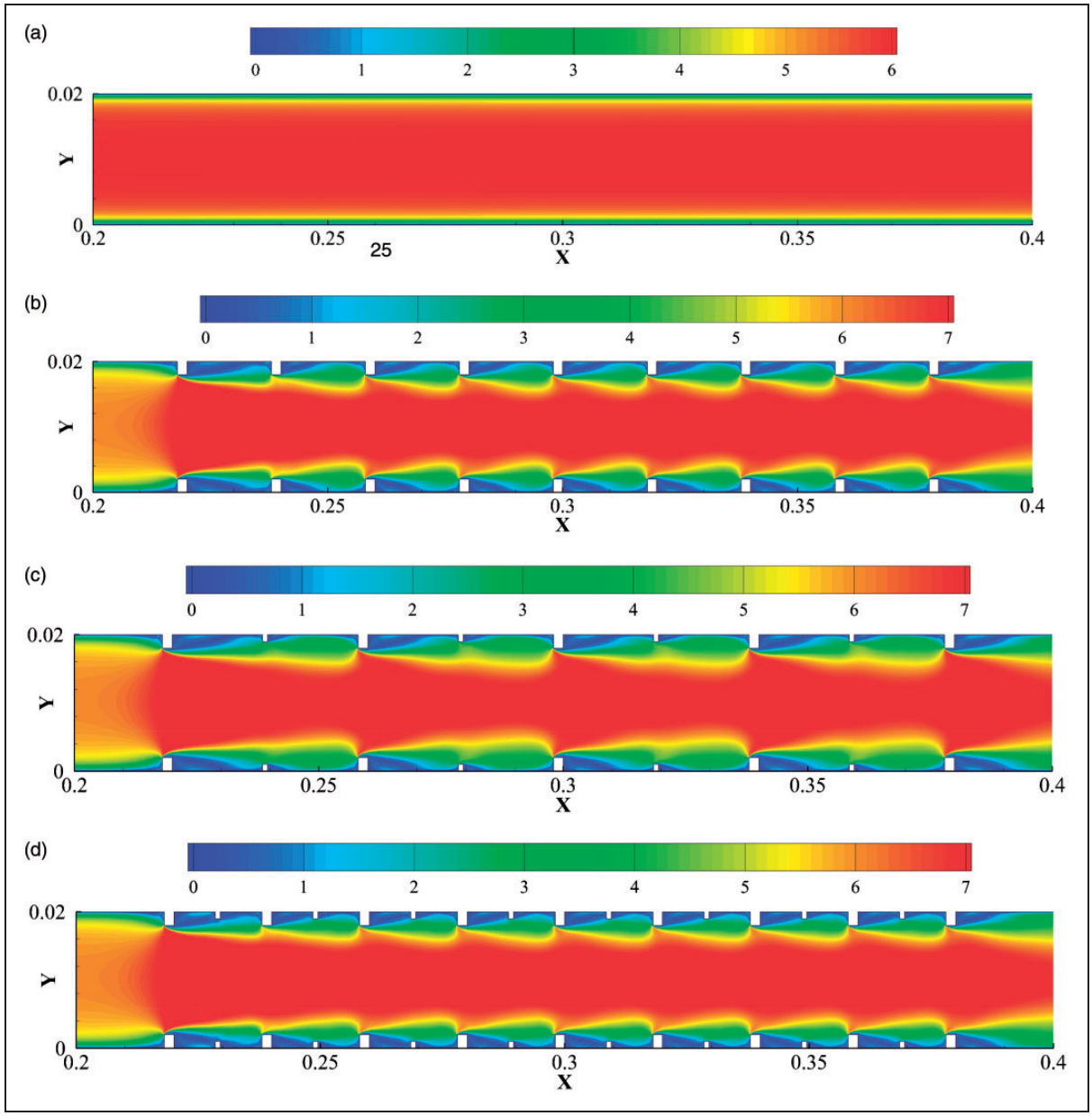

Figure 3. Air velocity fields for smooth, same-size and hybrid-size ribbed ducts. (a) Smooth-wall duct, (b) ribbed-wall duct, case A, (c) ribbed-wall duct, case B, (d) ribbed-wall duct, case C.

where J represents the particle number of deposition per unit time and unit surface area. C_0 represents the particle mean concentration. The particle deposition velocity is non-dimensionalized by the friction velocity u^* and is defined by equation (19)

$$V_d^+ = \frac{V_d}{u^*} = \frac{V_d}{\sqrt{\tau_w/\rho_g}} = \frac{V_d}{U_{mean}\sqrt{f/2}} \tag{19}$$

From Figure 5, the present dimensionless particle deposition velocity profile is in good agreement with the literature data. The particle deposition can be divided into the eddy diffusion-impaction regime and inertia-moderated regime within the particle size range considered by this study. In the eddy diffusion-impaction regime, turbulent eddy diffusion and particle inertia are the main influencing factors to control the particle deposition process. The deposition velocity would be greatly increased with the particle relaxation time for several orders of magnitudes. In the inertia-moderated regime, the particle deposition behaviours are mainly determined by the inertia of the particles, and the particle deposition velocity almost keeps constant with the increase of

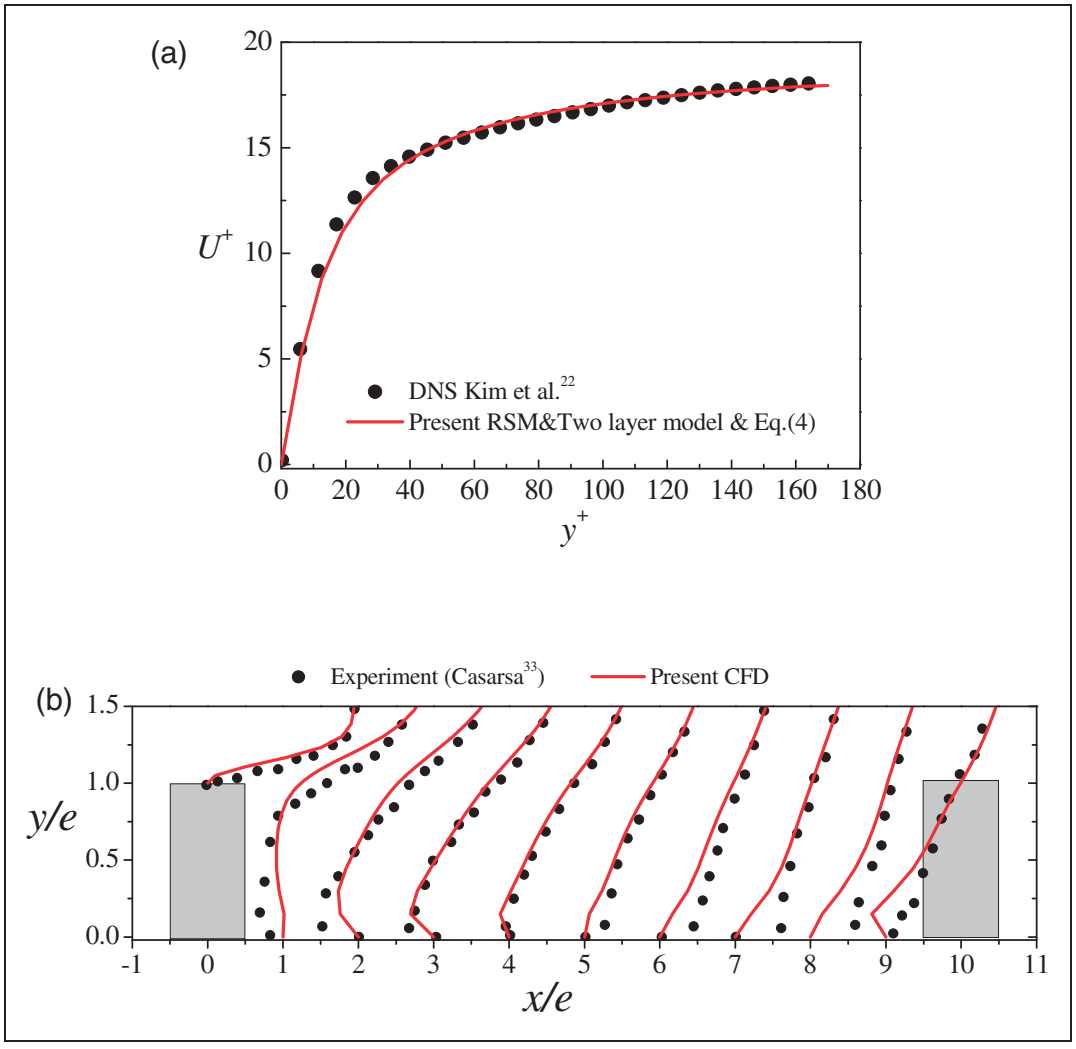

Figure 4. Validation of air velocity profiles for smooth duct case and ribbed duct case A. (a) Smooth wall (b) ribbed duct case A.

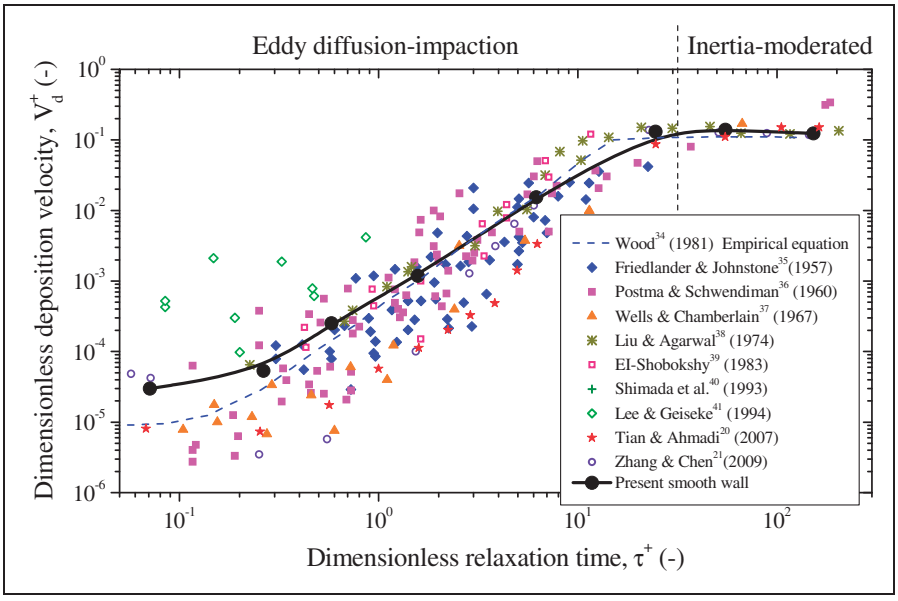

Figure 5. Validation of particle deposition velocity in smooth duct air flow.

particle relaxation time. The two particle deposition regimes can be well predicted in present simulation, as shown in Figure 5. The agreements of the air flow velocity profiles as well as the particle deposition velocity profile indicate that the present CFD model and solution strategy can simulate the particle deposition in both smooth and ribbed duct air flows.

Particle deposition enhancement by hybrid-size surface ribs

The particle deposition velocity profiles for smooth and ribbed duct cases were displayed in Figure 6. Obviously, the particle deposition velocities were shown to become significantly increased due to the arrangement of surface ribs. Moreover, the deposition enhancement ratios are significantly different for different particle sizes. The particle deposition velocity can be enhanced for three or four orders of magnitude for small particles ($\tau_p^+ < 1$), while for large particles ($\tau_p^+ > 1$), one or two orders of magnitude increase was shown. As complicated turbulent vortices are induced by the disturbance of surface ribs, small particles can be easily captured by the near-wall turbulent eddies and entrained to the walls and rib surfaces for deposition, while the motion trajectories of large particles are hardly influenced by the turbulent vortices for their large inertia. In the logarithmic coordinates, as shown in Figure 6, the difference of particle deposition velocities among the three types of ribbed duct cases is not obvious. To clearly and quantitatively observe the deposition enhancement ratio for the ribbed duct cases, an enhanced ratio $\gamma = v_{drough}/v_{dsmooth}$ was defined and depicted in Figure 7. The $v_{dsmooth}$ and v_{drough} are the dimensional particle deposition velocities for smooth and ribbed duct cases, respectively. The simulation results from our previous study[14] were also compared with the present simulation, as shown in Figure 7. The ribbed case D is $e/D = 0.05$ and $p/e = 10$, while the ribbed case E is $e/D = 0.1$, $p/e = 6$. From Figure 7, the particle deposition enhancement by all kinds of surface ribs is not obvious for large particles ($\tau_p^+ > 1$). Moreover, the difference of particle deposition enhancement ratios is slight for different surface ribs. The maximum enhancement ratio cannot exceed 500 for large particles. Nevertheless, the hybrid-size surface ribs with rib spacing $p/e = 5$ (ribbed case C) was shown to have the best performance on particle deposition velocity enhancement for small particles ($\tau_p^+ < 1$), compared with the other surface rib height and spacing. The maximum enhanced ratio can reach 4700 for 1 μm particles. In our previous study,[14] the deposition mechanism for small particles was found to be mainly due to the interception of windward surfaces of ribs, the increase of deposition area and the captures and entrainment of turbulent eddies. The largest T.K.E distribution in the near-wall region occurs for the ribs spacing $p/e = 10$.[14] The T.K.E values and the momentum exchange between the rib cavity and the outer flow would be reduced with a decrease reduction in the rib spacing.[14] For the ribbed case C, the spacing is between two larger surface ribs that are kept to $p/e = 10$. The flow structures and the T.K.E distributions would not be essentially modified by the smaller ribs that are arranged between the nearby larger ribs. Nevertheless, the interception of windward surface and the area of deposition are enhanced by the small surface ribs. Therefore, the deposition enhancement would reach maximum for ribbed case C. For ribbed case E, the rib spacing $p/e = 6$. The first two deposition mechanisms are enhanced, while T.K.E values are reduced due to the flow structures. For the ribbed case D, the surface rib

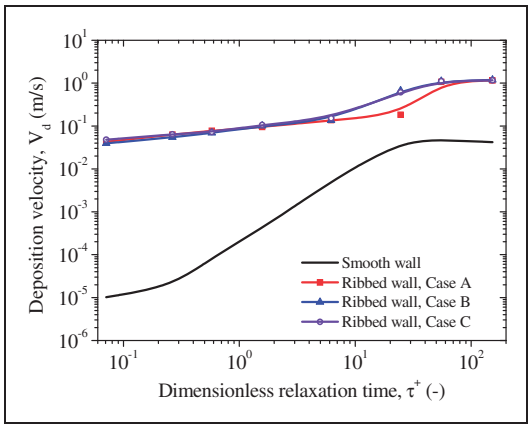

Figure 6. Particle deposition velocities for smooth, same-size and hybrid-size ribbed duct cases.

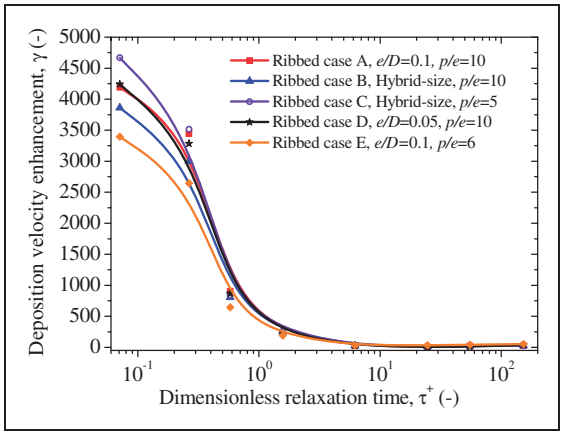

Figure 7. Particle deposition enhancement ratios by same-size and hybrid-size ribbed ducts.

is too small. Thus, the first two deposition mechanisms are weakened. Therefore, the ribbed case C has the best enhancement performance on particle deposition for small particles.

Particle deposition efficiency ratio

Our simulation results have shown that surface ribs can greatly enhance particle deposition rate. Nevertheless, the ribs were also shown to enhance the flow drag. Therefore, it is necessary to evaluate the comprehensive performance of different types of surface ribs on the particle deposition efficiency. An efficiency ratio of particle deposition enhancement was defined by equation (20) as follows

$$\eta = \frac{v_{drough}}{v_{dsmooth}} \cdot \frac{\mathrm{f}_{smooth}}{\mathrm{f}_{rough}} \tag{20}$$

where f_{smooth} and f_{rough} are the flow drags for smooth and ribbed duct cases, respectively. The flow drag of the second half duct for the smooth duct case is 0.0732 N, while they are 0.72006, 0.5853 and 0.7034 for the ribbed duct cases A, B and C, respectively. Thus, the increased ratios of flow resistance are 9.8, 8.0 and 9.6 for the three ribbed duct cases respectively, as shown in Table 2. The flow drags between cases A and C are very similar. It means that the flow resistance is mainly controlled and produced by large surface ribs. For case B, the low flow drag compared with ribbed case A and C is favourable for improving the comprehensive particle deposition efficiency.

Figure 8 shows the efficiency ratios η for the three ribbed duct cases. Significant differences were shown between same-size and hybrid-size surface ribs for small particles ($\tau_p^+ < 1$), considering the flow drag increase. The maximum efficiency ratio can reach 485 for the two hybrid-size rib cases when particle size is 1 μm, while it is 425 for the same-size rib case. The efficiency ratio is increased for about 14% by the hybrid-size ribs, compared with the same-size rib case. Almost no differences can be found between the two hybrid-size ribbed duct cases. Because the flow drag increase is lower for the ribbed duct case B, while the ribbed duct case C has better performance on particle deposition enhancement. For large particles ($\tau_p^+ > 1$), the efficiency ratios are almost the same for the three ribbed duct cases. This is because the turbulent vortices and flow structures modified by the surface ribs have little effects on large particle movements. As a whole, the hybrid-size surface ribs can enhance the particle deposition better than the same-size ones, and the particle deposition enhancement by surface ribs is effective for small particles ($\tau_p^+ < 1$).

Table 2. Flow drags for smooth, same-size and hybrid-size ribbed duct cases.

Case No.	Case S	Case A	Case B	Case C
Flow drag (N)	0.0732	0.7206	0.5853	0.7034
Increased ratio	–	9.8	8.0	9.6

Mechanisms of particle deposition enhancement

The particle deposition enhancement is induced by the following three mechanisms: the interception of windward surfaces of ribs, the increase of deposition area and the captures and entrainment of turbulent eddies induced by the repeated surface ribs.

Firstly, for the interception of windward surface of ribs, the windward area of surface ribs is crucial for particle deposition enhancement. The windward areas of ribs were calculated for ribbed duct cases A, B and C and these are respectively 0.036, 0.028 and 0.052 m in 2D. The ribbed case C has the largest windward area to intercept particles to deposition. Secondly, the particle deposition area is obviously increased by the surface ribs. A large number of particles would be deposited on the rib surfaces. The total deposition area is 0.4 m for the smooth duct case. Nevertheless, for ribbed duct cases A, B and C, the deposition area can be 0.472, 0.456, and 0.504 m respectively. Therefore, the increase ratios of deposition areas are 18%, 14% and 26% for the three ribbed duct cases, respectively. Obviously, arrangement of more surface ribs on the walls can provide larger windward surface areas and total deposition areas. The ribbed duct case C has larger

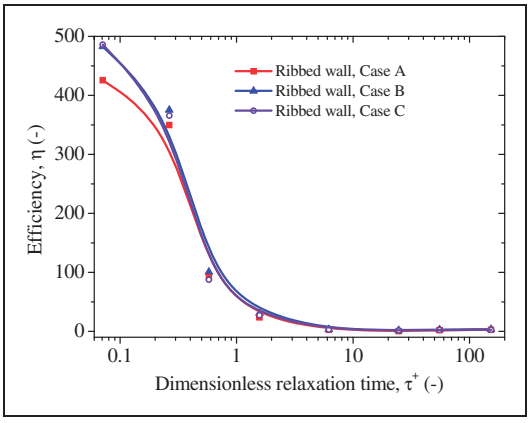

Figure 8. Efficiency ratio of particle deposition enhancement.

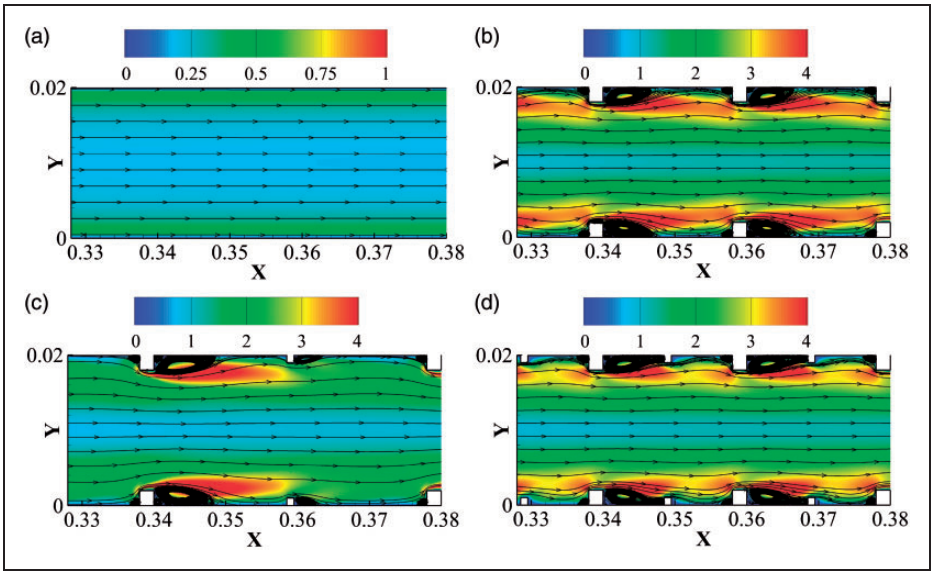

Figure 9. T.K.E distribution and streamlines of turbulent air flow for smooth, same-size and hybrid-size ribbed duct cases. (a) Smooth-wall duct, (b) ribbed-wall duct, case A, (c) ribbed-wall duct, case B (d) ribbed-wall duct, case C.

number of ribs and is beneficial for particle deposition enhancement due to the above two mechanisms. These are the main mechanisms to enhance deposition for large particles ($\tau_p^+ > 1$).

For small particles ($\tau_p^+ < 1$), the third mechanism is important to lead to particle deposition enhancement. To clearly present the role of turbulent eddies on particle deposition, Figure 9 displays the T.K.E. distribution and streamlines of turbulent air flow for smooth, same-size and hybrid-size ribbed duct cases. Compared with the smooth duct case, the flow structures are quite complex for ribbed duct flow. A large number of turbulent eddies are produced in the cavities and intense T.K.E. distributions are induced in the near-wall regions, as shown in the red areas in Figure 9(b) to (d). Small particles would be easily captured by the turbulent vortices and entrained into the recirculation region for deposition, once they move into the near-wall regions. These are much favourable for particle turbulent deposition with small particle sizes, which is the reason that surface ribs have much better performance for small particles than those for large particles. Compared with the three ribbed duct cases, more turbulent eddies and larger T.K.E. regions are induced for the ribbed case C. Therefore, the ribbed case C has the best deposition enhancement performance in the three ribbed cases. The enhancement mechanisms for ribbed case B are the weakest. However, considering the flow drag, the hybrid-size ribbed cases B and C have almost the same efficiency ratio for particle deposition enhancement, which are better than the same-size ribbed duct case. Therefore, the hybrid-size ribbed surfaces are recommended to apply in the air clean devices for particle deposition enhancement.

Conclusions

Particle deposition enhancement by same-size and hybrid-size surface ribs in turbulent air duct flows were numerically investigated by CFD simulation with RSM and DPM model. The UDF corrections were made to improve the simulation results and accuracy. The simulation results were firstly validated well with the literature results, and then the particle deposition enhancement ratios and mechanisms and flow drag increase were studied and analysed in detail. The following conclusions are drawn:

1. The hybrid-size ribs with small rib spacing (ribbed case C) have the best performance on particle deposition enhancement for small particles ($\tau_p^+ < 1$). The maximum enhancement ratio can be 4700 for 1 μm particles. While no obvious particle deposition enhancement can be found for large particles ($\tau_p^+ > 1$) for the three types of surface ribs.
2. For the flow drag increase, the lowest flow drag appears for the hybrid-size ribs with large rib spacing (ribbed case B). Besides, the hybrid-size ribbed case, C has almost the same flow drag with the same-size ribbed case A.
3. The comprehensive deposition efficiency ratios for hybrid-size surface ribs are significantly higher than same-size ones for small particles ($\tau_p^+ < 1$). It can reach 485 for 1 μm particles for ribbed case B and

C. However, for large particles ($\tau_p^+ > 1$), the efficiency ratios are less than three for all the ribbed ducts.

Therefore, the hybrid-size surface ribs are more effective and efficient for particle deposition enhancement with the same flow drag, compared with the same-size ribs.

In future work, the three-dimensional simulation will be conducted and the influences of particle-wall impaction as well as particle re-suspension can be considered and evaluated.

Authors' contributions

All authors contributed equally in the preparation of this manuscript.

Declaration of conflicting interests

The author(s) declared no potential conflicts of interest with respect to the research, authorship and/or publication of this article.

Funding

The author(s) disclosed receipt of the following financial support for the research, authorship, and/or publication of this article: The authors appreciate the financial supports provided by The Hong Kong Polytechnic University Postdoctoral Fellowships Scheme (G-YW0K) and Central Policy Unit of the Hong Kong Government via the Public Policy Research Scheme (2013.A6.010.13A).

References

1. Zhang JP and Li AG. Study on particle deposition in vertical square ventilation duct flows by different models. *Energ Convers Manage* 2008; 49: 1008–1018.
2. Gao R and Li AG. Dust deposition in ventilation and air-conditioning duct bend flows. *Energ Convers Manage* 2012; 55: 49–59.
3. Vincent JH and MacLennan ASM. Aerodynamic considerations in electrostatic precipitator. *J Electrostatic* 1980; 8: 325–342.
4. Lai ACK, Byrne MA and Goddard AJH. Measured deposition of aerosol particles on a two-dimensional ribbed surface in a turbulent duct flow. *J Aerosol Sci* 1999; 30: 1201–1214.
5. Lai ACK, Byrne MA and Goddard AJH. Aerosol deposition in turbulent channel flow in a regular array of three dimensional roughness elements. *J Aerosol Sci* 2001; 32: 121–137.
6. Barth T, Reiche M, Banowski M, et al. Experimental investigation of multilayer particle deposition and resuspension between periodic steps in turbulent flows. *J Aerosol Sci* 2013; 64: 111–124.
7. Chen Q. Ventilation performance prediction for buildings: a method overview and recent applications. *Build Environ* 2009; 44: 848–858.
8. Jiang H, Lu L and Sun K. Simulation of particle deposition in ventilation duct with a particle-wall impact model. *Build Environ* 2010; 45: 1184–1191.
9. Sun K, Lu L and Jiang H. A computational investigation of particle distribution and deposition in a 90 °bend incorporating a particle-wall model. *Build Environ* 2011; 46: 1251–1262.
10. Suh YJ and Kim SS. Effect of obstructions on the particle collection efficiency in a two-stage electrostatic precipitator. *J Aerosol Sci* 1996; 27: 61–74.
11. Iacono GI, Tucker P and Reynolds A. Predictions for particle deposition from LES of ribbed channel flow. *Int J Heat Fluid Flow* 2005; 26: 558–568.
12. Lecrivain G, Drapeau-Martin S, Barth T, et al. Numerical simulation of multilayer deposition in an obstructed channel flow. *Adv Powder Technol* 2014; 25: 310–320.
13. Lu H and Lu L. Numerical investigation on particle deposition enhancement in duct air flow by ribbed wall. *Build Environ* 2015; 85: 61–72.
14. Lu H and Lu L. Effects of rib spacing and height on particle deposition in ribbed duct air flows. *Build Environ* 2015; 92: 317–327.
15. Lu H and Lu L. A numerical study of particle deposition in ribbed duct flow with different rib shapes. *Build Environ* 2015; 94: 43–53.
16. Lu H and Lu L. CFD investigation on particle deposition in aligned and staggered ribbed duct air flows. *Appl Therm Eng* 2016; 93: 697–706.
17. Xie GN, Zheng SF, Zhang WH, et al. A numerical study of flow structure and heat transfer in a square channel with ribs combined downstream half-size or same-size ribs. *Appl Therm Eng* 2013; 61: 289–300.
18. FLUENT Inc. *FLUENT 12.0 user's guide*. Lebanon, NH: Author, 2009.
19. Chen HC and Patel VC. Near-wall turbulence models for complex flows including separation. *AIAA J* 1988; 26: 641–648.
20. Tian L and Ahmadi G. Particle deposition in turbulent duct flows-comparisons of different model predictions. *J Aerosol Sci* 2007; 38: 377–397.
21. Zhang Z and Chen Q. Prediction of particle deposition onto indoor surfaces by CFD with a modified Lagrangian method. *Atmos Environ* 2009; 43: 319–328.
22. Kim J, Moin P and Moser R. Turbulence statistics in fully developed channel flow at low Reynolds number. *J Fluid Mech* 1987; 177: 133–166.
23. Gao NP and Niu JL. Modeling particle dispersion and deposition in indoor environments. *Atmos Environ* 2007; 41: 3862–3876.
24. Gao N, Niu J, He Q, et al. Using RANS turbulence models and Lagrangian approach to predict particle deposition in turbulent channel flows. *Building Environ* 2012; 48: 206–214.
25. Zhao B, Zhang Y, Li XT, et al. Comparison of indoor aerosol particle concentration and deposition in different ventilated rooms by numerical method. *Building Environ* 2004; 39: 1–8.
26. Zhao B and Chen JJ. Numerical analysis of particle deposition in ventilation duct. *Building Environ* 2006; 41: 710–718.
27. Zhao B, Chen C, Yang XY, et al. Comparison of three approaches to model particle penetration coefficient through a single straight crack in a building envelope. *Aerosol Sci Technol* 2010; 44: 405–416.
28. Zhou B, Zhao B and Tan ZC. How particle resuspension from inner surfaces of ventilation ducts affects indoor air quality – a modeling analysis. *Aerosol Sci Technol* 2011; 45: 996–1109.
29. Jin HH, Fan JR, Zeng MJ and Cen KF. Large eddy simulation of inhaled particle deposition within the human upper respiratory tract. *J Aerosol Sci* 2007; 38: 257–268.
30. Jin HH, He C, Lu L and Fan JR. Numerical investigation of the wall effect on airborne particle dispersion in a test chamber. *Aerosol Air Qual Res* 2013; 13: 786–794.
31. Jiang H, Lu L and Sun K. Experimental study and numerical investigation of particle penetration and deposition in 90 degrees bent ventilation ducts. *Build Environ* 2011; 46: 2195–2202.
32. Partankar SV. *Numerical heat transfer and fluid flow*. Hemisphere, Washington, DC, 1980.

33. Casarsa L. *Aerodynamic performance investigation of a fixed rib-roughened internal cooling passage*. PhD Thesis, Von Karman Institute for Fluid Dynamics, Sint-Genesius-Rode, Belgium; 2003.
34. Wood NB. A simple method for the calculation of turbulent deposition to smooth and rough surfaces. *J Aerosol Sci* 1981; 12: 275–290.
35. Friedlander SK and Johnstone HF. Deposition of suspended particles from turbulent gas streams. *Ind Eng Chem* 1957; 49: 1151–1156.
36. Postma AK and Schwendiman LC. *Studies in micrometrics: I. Particle deposition in conduits as a source of error in aerosol sampling*. Report HW-65308. Richland, Washington: Hanford Laboratory, 1960.
37. Wells AC and Chamberlain AC. Transport of small particles to vertical surfaces. *Br J Appl Phys* 1967; 18: 1793–1799.
38. Liu BYH and Agarwal JK. Experimental observation of aerosol deposition in turbulent flow. *J Aerosol Sci* 1974; 5: 145–155.
39. El-Shobokshy MS. Experimental measurements of aerosol deposition to smooth and rough surfaces. *Atmos Environ* 1983; 17: 639–644.
40. Shimada M, Okuyama K and Asai M. Deposition of submicron aerosol particles in turbulent and transitional flow. *AICHE J* 1993; 39: 17–26.
41. Lee KW and Gieseke JA. Deposition of particles in turbulent pipe flows. *J Aerosol Sci* 1994; 25: 699–709.